Biochemistry

pubs.acs.org/biochemistry Article

Structural and Biochemical Characterization of MppQ, an L-Enduracididine Biosynthetic Enzyme from *Streptomyces hygroscopicus*

Nemanja Vuksanovic,[⊥] Trevor R. Melkonian,[⊥] Dante A. Serrano, Alan W. Schwabacher, and Nicholas R. Silvaggi*

Cite This: *Biochemistry* 2023, 62, 3105−3115 Read Online

ACCESS | Metrics & More | Article Recommendations | Supporting Information

ABSTRACT: MppQ is an enzyme of unknown function from *Streptomyces hygroscopicus* (ShMppQ) that operates in the biosynthesis of the nonproteinogenic amino acid L-enduracididine (L-End). Since L-End is a component of several peptides showing activity against antibiotic-resistant pathogens, understanding its biosynthetic pathway could facilitate the development of chemoenzymatic routes to novel antibiotics. Herein, we report on the crystal structures of ShMppQ complexed with pyridoxal-5′-phosphate (PLP) and pyridoxamine-5′-phosphate (PMP). ShMppQ is similar to fold-type I PLP-dependent aminotransferases like aspartate aminotransferase. The tertiary structure of ShMppQ is composed of an N-terminal extension, a large domain, and a small domain. The active site is placed at the junction of the large and small domains and includes residues from both protomers of the homodimer. We also report the first functional characterization of MppQ, which we incubated with the enzymatically produced 2-ketoenduracidine and observed the conversion to L-End, establishing ShMppQ as the final enzyme in L-End biosynthesis. Additionally, we have observed that MppQ has a relatively high affinity for 2-keto-5-guanidinovaleric acid (i.e., 2-ketoarginine), a shunt product of MppP, indicating the potential role of MppQ in increasing the efficiency of L-End biosynthesis by converting 2-ketoarginine back to the starting material, L-arginine. A panel of potential amino-donor substrates was tested for the transamination activity against a saturating concentration of 2-ketoarginine in end-point assays. Most L-Arg was produced with L-ornithine as the donor substrate. Steady-state kinetic analysis of the transamination reaction with L-Orn and 2-ketoarginine shows that the kinetic constants are in line with those for the amino donor substrate of other fold-type I aminotransferases.

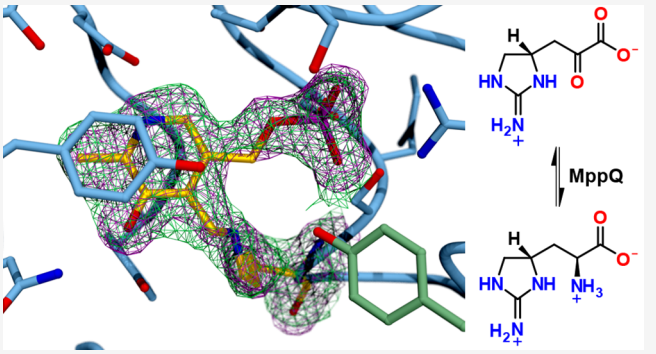

INTRODUCTION

Antibiotic-resistant pathogens are a continuing threat to public health. Mannopeptimycin from *Streptomyces hygroscopicus* and enduracidin from *S. fungicidicus* are nonribosomally produced peptide antibiotics with activity against a number of Gram-positive pathogens, including drug-resistant strains like methicillin-resistant *Staphylococcus aureus* (MRSA) and vancomycin-resistant enterococci (VRE).[1,2] Both of these agents were discovered decades ago, but despite their promising potency against problematic pathogens, poor aqueous solubility[3] or suboptimal activity/pharmacokinetics[4] have prevented their use in the clinic.

The search for optimized analogues of enduracidin and mannopeptimycin has been hampered by the difficulty of altering the core peptides of these antibiotics, since they both contain the unusual nonproteinogenic amino acid L-enduracididine (L-End, **1**; Scheme 1), or its hydroxylated derivative *β*-hydroxy L-enduracididine (*β*hEnd, **2**). This amino acid is not commercially available and, while synthetic routes have been developed,[5−7] they are multistep processes starting from advanced intermediates. The limited availability of this key building block has hampered efforts to make large groups of mannopeptimycin or enduracidin analogues. As a result, our understanding of the structure−activity relationships in these compounds is limited. A relatively inexpensive and facile route to L-End could facilitate the development of mannopeptimycin and enduracidin derivatives with improved therapeutic properties.

Feeding experiments with radio-labeled amino acids[8,9] showed that L-End biosynthesis originates with L-Arg (**3**).

Received: August 14, 2023
Revised: October 11, 2023
Accepted: October 13, 2023
Published: October 27, 2023

https://doi.org/10.1021/acs.biochem.3c00428
Biochemistry 2023, 62, 3105−3115

Scheme 1. Mannopeptimycin and Enduracidin Derivatives

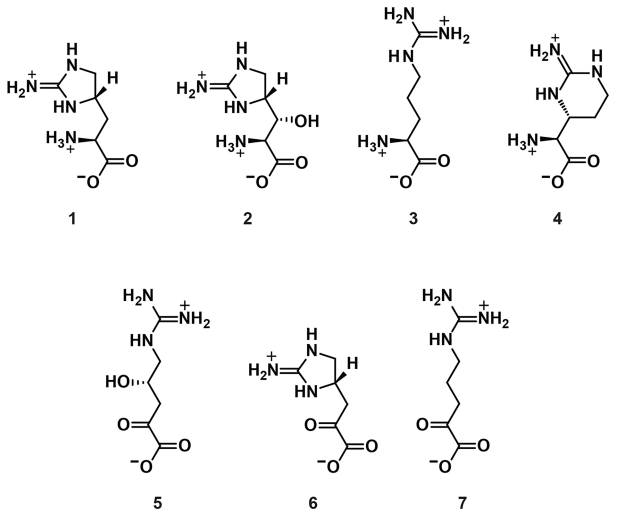

The biosynthetic clusters for both mannopeptimycin and enduracidin have been characterized,[2,10] and they share only three genes in common: *mpp/endP*, *Q*, and *R*. Disruption of any of these genes in *S. fungicidicus* abrogates the production of enduracidin. This defect can be rescued by the addition of exogenous L-End to the growth medium.[11] Thus, the Mpp/EndPQR gene products appear to convert L-Arg to L-End in the biosynthesis of mannopeptimycin and enduracidin, respectively. The mystery of how these three gene products produce L-End was only deepened by comparison to the biosynthetic pathway of a related, arginine-derived non-proteinogenic amino acid, L-capreomycidine (**4**).

Capreomycidine, a component of the antibiotic viomycin, is structurally similar to L-End and is produced by a two-enzyme system. VioC is a nonheme iron- and α-ketoglutarate-dependent oxygenase that hydroxylates L-Arg at the β-carbon atom.[12] VioD is a fold-type I PLP-dependent aminotransferase that catalyzes a unique intramolecular aminotransfer reaction that leads to the pyrimidinyl ring of **4**.[13] This system uses one enzyme to activate the β-carbon for cyclization and a second enzyme to create the ring. L-End biosynthesis, in contrast, requires three enzymes. Two of these are PLP-dependent enzymes that could be capable of catalyzing the cyclization step (MppP and MppQ), and none of the three was expected, on the basis of amino acid sequence analysis, to possess the catalytic capacity to activate the γ-carbon atom for cyclization.

The sequence of chemical steps leading from L-Arg to L-End and the intermediates involved became clearer when it was found that MppP from *S. wadayamensis* (SwMppP; a close homologue of the *S. hygroscopicus* enzyme and also in a mannopeptimycin biosynthetic cluster) is a novel type of PLP-dependent oxidase that catalyzes the oxidation of L-Arg to 2-oxo-4-hydroxy-5-guanidinovaleric acid (**5**).[14,15] This observation fits in well with the previous work on MppR from *S. hygroscopicus* (ShMppR) that indicated that this enzyme can operate on an oxidized arginine derivative like **5** to produce the ketone form of L-End (**6**).[16] SwMppP also generates the partially oxidized, abortive product 2-oxo-5-guanidinovaleric acid (**7**) about 35% of the time in vitro. It is not known if **7** is also produced in vivo.[14,15]

The PLP-dependent enzymes are a large group of proteins that catalyze a wide range of reactions, including racemization, decarboxylation, β- and γ-substitution/elimination, and transamination.[17,18] The transamination reaction is prevalent among PLP-dependent enzyme activities, with 124 Enzyme Commission classifications (2.6.1.1−124). Herein we report the X-ray crystal structure of *S. hygroscopicus* MppQ (ShMppQ), which shows that this enzyme is a typical fold-type I[19−21] aminotransferase, matching both the tertiary structure and active site architecture of well characterized aminotransferases like aspartate aminotransferase from *E. coli* (EcAAT)[22,23] and human kynurenine aminotransferase II (hKAT).[24]

Steady-state kinetic analysis of the transamination reaction between the potential substrate **7** and L-Ala showed that the structural similarities are not coincidental; ShMppQ catalyzes the aminotransfer reaction. Preliminary kinetic studies involving its physiological substrate, **6**, and L-alanine confirm the role of MppQ as a bona fide aminotransferase in the L-End pathway (Scheme 2). Based on the results of mass spectrometry-based end-point assays, we have identified L-ornithine and L-Gln as potential amino group donor substrates. These studies suggest that ShMppQ catalyzes the conversion of 2-ketoenduracididine to L-End, completing our understanding of L-End biosynthesis.

MATERIALS AND METHODS

Protein Expression and Purification. The gene encoding *S. hygroscopicus* MppQ (UniProt accession code Q643B9) was synthesized by GenScript, Inc. and subcloned into the pE-SUMO$_{kan}$ vector for expression in *E. coli* BL21 Star cells. Transformed cells were grown at 37 °C in 2−4 L of Luria−

Scheme 2. Role of MppQ as a Bona Fide Aminotransferase in the L-End Pathway

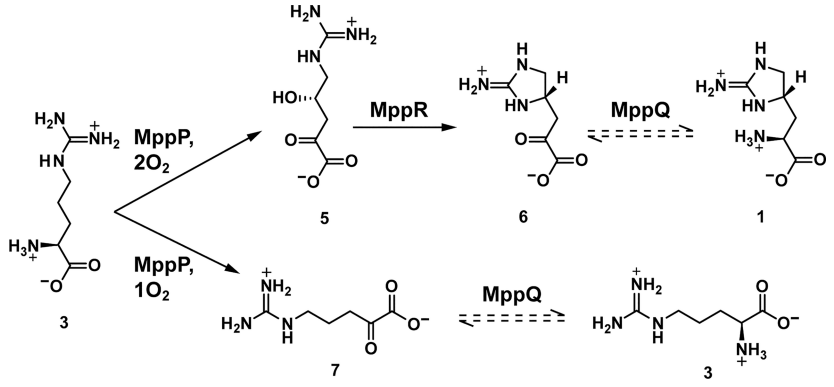

https://doi.org/10.1021/acs.biochem.3c00428
Biochemistry 2023, 62, 3105−3115

Bertani medium containing 50 μg mL^{-1} kanamycin to an $OD_{600\ nm}$ of ∼1.0. The expression of MppQ was induced with 0.4 mM isopropyl β-D-1-thiogalactopyranoside (IPTG), and the temperature was reduced to 25 °C. After 18 h, the cells were harvested by centrifugation at 5400g for 30 min. The pellets, approximately 10 g L^{-1} of culture, were resuspended in 5 mL of buffer A (25 mM TRIS, pH 8.0, 300 mM NaCl, 10 mM imidazole, 200 μM PLP) per gram of cell pellet. The cells were lysed in a circulating ice bath using a Fisher Scientific Model 500 sonic dismembrator at 70% amplitude, for a total of 10 min (20 pulses of 30 s each, separated by 1 min rest periods). The resulting lysate was clarified by centrifugation at 39,000g (18,000 rpm) for 1 h. The clarified lysate was passed through a 0.45 μm syringe filter and loaded in 30 mL aliquots onto a 5 mL HisTrap FF column (Cytiva) that had been pre-equilibrated with buffer A (without PLP). After washing with 10 column volumes of buffer A, the protein was washed further and ultimately eluted using a step gradient at 10, 50, and 100% buffer B (25 mM TRIS at pH 8.0, 300 mM NaCl, and 250 mM imidazole). Fractions containing significant amounts of SUMO-MppQ, as judged by a Coomassie-stained SDS-PAGE gel, were pooled, and His_6-Ulp1 protease was added to a final concentration of 2.0 μM. The pooled HisTrap fractions were dialyzed overnight at 4 °C against 3.5 L of buffer C (50 mM TRIS pH 8.0, 150 mM NaCl, 0.5 mM DTT). The following day, the cleaved His_6-SUMO tag and protease were removed by passing the dialysate over the HisTrap FF column a second time. The flow-through fractions were collected and judged to be >95% pure by SDS-PAGE. The protein concentration was quantified by $A_{280\ nm}$ using the calculated extinction coefficient of 37150 M^{-1} cm^{-1}. The protein was dialyzed against 3.5 L of storage buffer (20 mM TRIS pH 8.0, 200 μM PLP) overnight at 4 °C, then concentrated to 11−15 mg mL^{-1}, and used directly or mixed 1:1 with glycerol (50%) and snap-frozen in liquid nitrogen.

Crystallization. Crystals of ShMppQ·PLP (internal aldimine) were grown by the hanging-drop vapor diffusion method over wells containing 15−25% PEG 3350 and 0.1−0.2 M ammonium citrate trihydrate, trilithium citrate, or ammonium sulfate. Crystals appeared as clusters of thin needles after 3−7 days. The size and morphology of the crystals were improved by microseeding. The crystal used for the MppQ·PMP structure was grown as above, except that the well solution contained 100 mM L-arginine, pH 8.0. Crystals were cryoprotected for data collection by soaking briefly in a sequence of solutions containing 30% PEG 3350, 0.2 M ammonium citrate trihydrate, and 5, 10, or 20% glycerol.

Data Collection and Processing. An initial data set was collected from a crystal of the MppQ holoenzyme at 100 K on beamline 21-ID-D of the Advanced Photon Source (Life Science Collaborative Access Team, LS-CAT) equipped with a MAR 300 CCD detector, using an oscillation angle of 1.0° over a total of 180° with an exposure time of 1 s, a crystal-to-detector distance of 250 mm, and wavelength of 0.97625 Å. Diffraction images were processed using iMOSFLM,[25] POINTLESS,[26] and SCALA,[26] as implemented in the CCP4 suite v.7.0.[27] This MppQ crystal diffracted to 2.1 Å resolution. A higher-resolution data set was collected from a different crystal, also at the LS-CAT beamline 21-ID-D, using an oscillation angle of 0.5° over a total of 140° at a distance of 220 mm. The exposure time and wavelength were the same as those for the first data set. This crystal was essentially identical to the initial one but was larger and diffracted to 1.8 Å resolution. These data were also processed using iMOSFLM, POINTLESS, and SCALA. The final data set reported here was collected at LS-CAT beamline 21-ID-G equipped with a MAR 300 CCD detector from an MppQ·L-Arg cocrystal. The X-ray wavelength was fixed at 0.97856 Å, the oscillation range was 0.5° over a total of 120°, the distance was 220 mm, and the exposure time was 1 s. This cocrystal diffracted to 1.6 Å resolution. These data were processed with autoPROC (Global Phasing, Ltd.).[28] Data processing statistics are listed in Table 1.

Table 1. Crystallographic Data Collection and Refinement Statistics of MppQ·PLP and MppQ·PMP

	MppQ·PLP	MppQ·PMP
PDB accession code	8TN2	8TN3
data collection		
space group	$P\ 2_12_12_1$	$P\ 2_1$
unit cell dimensions (Å)	47.73, 114.50, 133.32	47.77, 94.07, 84.29
unit cell angles (°)	90, 90, 90	90, 95.11, 90
resolution (Å)[a]	35.10−1.75 (1.81−1.75)	43.07−1.63 (1.69−1.63)
R_{symm}[b]	0.120 (0.665)	0.078 (0.451)
R_{meas}	0.132 (0.734)	0.090 (0.522)
R_{pim}	0.054 (0.306)	0.046 (0.262)
$CC_{1/2}$	0.995 (0.765)	0.996 (0.859)
$\langle I/\sigma(I)\rangle$	10.1 (2.5)	9.9 (3.0)
completeness (%)	97.4 (93.0)	97.1 (95.5)
multiplicity	5.5 (5.3)	3.9 (3.9)
no. of reflections	73,087 (6,815)	87,773 (4,602)
Wilson B-factor (Å^2)	12.8	15.0
model refinement		
R_{work}/R_{free}[c]	0.144/0.170	0.140/0.161
ave. B factors (non-H atoms; Å^2)[d]	17.3 (6,852)	22.2 (6,878)
protein	15.8 (5,936)	20.9 (6,021)
PLP/PMP	14.2 (30)	15.2 (32)
solvent	27.6 (886)	31.9 (825)
RMS deviations		
bond lengths (Å)	0.007	0.008
bond angles (deg)	0.85	1.002
coordinate error (Å)	0.15	0.14
Ramachandran statistics		
favored/allowed/outliers (%)	97.3/2.7/0.0	97.7/2.3/0.0
rotamer outliers (%)	0.17	0.33
cash score	2.34	4.20
number of TLS groups	8	6

[a]Values in parentheses relate to the highest resolution shell. [b]$R_{symm} = \Sigma\ |\ I - \langle I\rangle\ |/\Sigma\ I$, where I is the observed intensity and $\langle I\rangle$ is the average intensity from multiple measurements. [c]$R_{work} = \Sigma\ |F_o| - |\ F_c\ |/\Sigma\ |F_o|$ for reflections contained in the working set. R_{free} is calculated in the same manner using data from the test set (4.9% of the MppQ·PLP data set and 4.9% of the MppQ·PMP data set). [d]The average B factors reported are those calculated by phenix.model_vs_data and contain contributions from both local isotropic atomic vibrations and TLS motions.

Structure Determination and Model Refinement. Initial phases were obtained by molecular replacement using PHASER[29] (as implemented in the CCP4 suite v7.0) with the 2.1 Å resolution unliganded data set and the structure of *Pyrococcus horikoshii* OT3 kynurenine aminotransferase II (PDB ID 1 × 0 M;[24] 31% identical), with the 50 N-terminal residues, waters, and PLP-lysine removed. The lower

https://doi.org/10.1021/acs.biochem.3c00428
Biochemistry 2023, 62, 3105−3115

resolution data set was used for structure determination because the "*a*" cell edge of the crystal used to collect the 1.8 Å unliganded data set was oriented parallel to the spindle axis, resulting in poor sampling of the corresponding region of reciprocal space. The Matthews coefficient (V_M) of 2.21 Å^3 Da^{1-} (41% solvent) suggested that there were two molecules of MppQ (415 residues, 44.0 kDa) per asymmetric unit. While PHASER was able to find a viable solution (LLG = 33, TFZ = 9.5), it did not refine well. This poor molecular replacement model was subjected to density modification and automated rebuilding in PHENIX.AutoBuild[30−32] to remove bias and improve the model. PHENIX.AutoBuild resulted in a model with 761 residues (740 with side chains placed; ∼90% complete) in two chains, with R_{cryst} and R_{free} values of 20.0 and 24.0%, respectively. This model was used without refinement as the molecular replacement search model to obtain phases for the 1.8 Å resolution data set (LLG = 22,318; TFZ = 135). After iterative rounds of restrained refinement in PHENIX. Refine[33] and manual model building in COOT,[34,35] the final model of the PLP-bound, internal aldimine form of ShMppQ contained 2 molecules of MppQ (775 total residues), 846 water molecules, and 1 molecule of PLP per chain covalently bound at K250. The final R_{cryst} and R_{free} values were 14.4 and 17.0%, respectively.

The 1.6 Å resolution data from the MppQ·L-Arg cocrystal were phased by molecular replacement in PHASER using the MppQ·PLP structure as the search model (with waters and PLP removed and isotropic B-factors set to 20 Å^2; LLG = 20,477; TFZ = 6.7). After cycles of model building and refinement, the final model of the PMP-bound form of ShMppQ contained 2 molecules of MppQ (776 total residues), 825 water molecules, and 1 molecule of PMP per chain noncovalently bound near K250. The final R_{cryst} and R_{free} values were 14.0 and 16.1%, respectively.

Preparation of 6. The starting material for **6**, 4-(S)-hydroxy-2-ketoarginine (**5**), was produced enzymatically from L-Arg using arginine oxidase MppP. A reaction containing 100 mM L-Arg and 200 μM MppP was carried out in 20 mM ammonium acetate, pH 7.0. Bovine catalase (40 mg) was desalted in the reaction buffer (to remove the trehalose stabilizer that would complicate downstream NMR analysis) and added to the reaction mixture to prevent nonenzymatic oxidative decarboxylation of **5** by the hydrogen peroxide produced by MppP. The reaction was allowed to proceed overnight at 25 °C while shaking at 150 rpm. The reaction was quenched with 1 volume of methanol and centrifuged at 4000 rpm for 5 min to remove the precipitated enzyme. The supernatant was collected and evaporated to dryness at 50 °C in a Centrifan PE rotary evaporator. Approximately 1 mg of dried material was resuspended in approximately 1 mL of water, centrifuged at 13,000 rpm for 5 min to remove any particulates, and analyzed using a ZIC-HILIC column (3.5 μm, 100 Å, 50 × 2.1 mm) paired with a Shimadzu LC−MS/MS 8040 system. The mobile phase consisted of 20 mM ammonium formate, pH 4.0 (buffer A) and acetonitrile with 0.1% formic acid (buffer B). The liquid chromatographic separation was run at 0.5 mL/min and 35 °C; 15 μL of sample was injected. The following gradient program was used: hold at 90% B for 3.0 min, decrease to 40% B over 7 min, hold at 40% B for 2 min, increase to 90% B over 1 min, and hold at 90% B for 2 min. The sample was run in positive ESI mode, with a sprayer positioned at 4 mm. The dwell times for the fragmentation products of the 190 *m*/*z* precursor ion were set to 80 ms, while the dwell time for the 190 *m*/*z* parent ion was set to 247 ms.

The residue containing a mixture of **5** and **7** (Figure S1; 20 mg) was dissolved in a solution containing 180 μM MppR stored in 20 mM sodium phosphate, pH 7.5. The reaction was allowed to proceed for 2 h at 22 °C on a stir plate set at 100 rpm. The reaction was quenched with 1 volume of methanol and centrifuged at 4000 rpm for 5 min to remove the precipitated enzyme. The supernatant was collected and evaporated to dryness at 50 °C as before. The reaction products were analyzed using the same ZIC-HILIC column and a Shimadzu LC−MS/MS 8040 mass spectrometer. The same mobile phase was used. The analytes were eluted via gradient method at 0.5 mL/min and 35 °C. The injection volume was 0.5 μL. The following program was used in each run: hold at 90% B (3.0 min), decrease to 40% B (1.5 min), hold at 40% B (2 min), increase to 90% B (30 s), and hold at 90% B (2 min; 9 min total run time). The sample was run in positive ESI mode, with a sprayer positioned at 4 mm. The dwell time for the products of the 172, 162, and 144 *m*/*z* precursors was set to 100 ms (Figure S2).

Demonstration of ShMppQ Activity against 6. Snap-frozen ShMppQ stored in 50% glycerol, 25 mM TRIS, pH 8.5, 200 μM PLP was thawed, and glycerol was removed by buffer exchange with 20 mM TRIS, 200 μM PLP, pH 8.5 in a 10 kDa MWCO concentrator. The assay contained a nominal concentration of 50 μM **6**, 40 μM ShMppQ, and 100 mM L-Ala in 20 mM TRIS, pH 8.5, 200 μM PLP. The samples were manually quenched at 5, 10, 25, and 50 s using 1 volume of 0.1 M HCl. Measurements were conducted in triplicate. The reaction products were analyzed using a ZIC-HILIC column (3.5 μm, 100 Å, 50 × 2.1 mm) on a Shimadzu LC−MS/MS 8040 system using the 9 min gradient described previously. The injection volume was 25 μL for each sample; the dwell time of 172 and 173 *m*/*z* product ions was 100 ms.

Preparation of 7. The α-keto acid form of arginine was synthesized by enzymatic oxidation of L-arginine using a modified procedure developed by Meister[36] and a purification method developed by Stalon et al.[37] L-Arg (2 g, free base) was dissolved in 50 mL of water, and the pH was adjusted using hydrochloric acid to 7.1−7.3. Lyophilized bovine catalase (50 mg) was dissolved in 3 mL of 5 mM sodium phosphate, pH 7.5, followed by buffer exchange using a 10 kDa MWCO concentrator. The sample was concentrated back down to 3 mL. L-Amino acid oxidase (LAAO) from *Crotalus atrox* (60 mg of dried venom) was dissolved in 10 mL of water. One half of the catalase solution was added to the LAAO solution. The other half of the catalase solution was added to the L-Arg solution. The LAAO/catalase solution was then combined with the L-Arg/catalase solution, diluted to 100 mL with mqH_2O, and placed in a 1000 mL Erlenmeyer flask and covered loosely with foil. The reaction flask was placed in a shaking incubator at 25 °C, 100 rpm, in the dark for 16 h. The following day, the reaction was quenched with 100 mL of methanol and centrifuged at 4 °C and 3500 rpm for 10 min. The supernatant was collected. A 30 cm × 1 cm glass column was packed with 20 g of Dowex 50WX8 200−400 mesh in hydrogen form. A peristaltic pump set to a flow rate of 8 mL/min was used to pass 300 mL of 0.5 M NaOH over the Dowex resin, followed by 300 mL of 0.5 M HCl, 300 mL of 0.5 M NaCl, and finally 300 mL of water. The pH of water issued from the column must be 7.0 before the sample. The supernatant of the LAAO reaction was transferred to the

https://doi.org/10.1021/acs.biochem.3c00428
Biochemistry 2023, 62, 3105−3115

column, and the flow-through was collected in a round-bottom flask. The column was then washed with 500 mL of water, and the flow-through was collected in the same round-bottom flask. The flow-through was evaporated to dryness using a rotavap at 40 °C. Approximately 1 mg of sample was dissolved in 1 mL of deuterium oxide and centrifuged at 13,000 rpm for 5 min. The supernatant was collected, and 700 μL of it was loaded into an NMR tube. The sample was analyzed by ^{1}H, ^{13}C, and HSQC NMR. In aqueous solution, there are two forms of 7: linear and cyclic. In the cyclic form, the formation of a chiral center at C2 induces diastereotopic properties in the adjacent protons not seen in the linear form. In order to accurately integrate the spectrum, no standard such as acetonitrile was added as it would overlap with the peaks of interest. The shift alignment was therefore done using the water solvent peak as a reference (Figure S3). The solution should not be exposed to pH higher than 8.0 during purification as this will lead to aldol condensation between two 2-ketoarginine molecules, yielding a conjugated product with a purple color.

Assay of ShMppQ Activity against 7. The steady-state kinetics of ShMppQ-catalyzed transamination of L-Ala and 7 was studied by coupling the reaction to *E. coli* lactate dehydrogenase (EcLDH, EC 1.1.1.27). Pyruvate produced in the transamination reaction was reduced by EcLDH, resulting in a loss of absorbance at 340 nm due to the oxidation of NADH ($\varepsilon_{340\ nm}$ = 6220 M^{-1} cm^{-1}). The reactions contained 2 μM ShMppQ, 100 mM L-Ala, 20 U/mL EcLDH, 400 μM NADH, and concentrations of 7 ranging from 2.5−320 μM. The reaction was carried out in 50 mM bicine, 100 mM NaCl, 50 μM PLP, pH 7.8. The absorbance at 340 nm was monitored using an Evolution 300 UV−vis spectrophotometer (Thermo Scientific). The k_{cat} and K_M values were determined from the initial velocity data using eq 1, where S is the concentration of 7, v_0 is the initial velocity, V_M is the maximum velocity, and K_M is the Michaelis constant. Nonlinear regression analysis was performed with GraphPad Prism.

$$v_0 = \frac{V_M S}{(K_M + S)} \quad (1)$$

Amino Donor Substrate Screening. All reactions were carried out in 1 mL volumes containing 5 μM ShMppQ, 1 mM 7, and one of the 1 mM amino donor substrates in 50 mM bicine, 10 mM NaCl, and 50 μM PLP, pH 7.8. The candidate amino donor substrates were L-His, L-Gln, L-Orn, L-Lys, L-canavanine, L-Ala, L-Thr, L-Ile, L-Phe, L-Asp, and L-Glu. Samples of these reactions were quenched with an equal volume of acetonitrile after 5 and 10 min. Each reaction was run in triplicate. The reaction products were analyzed on a ZIC-HILIC column (3.5 μm, 100 Å, 50 × 2.1 mm) on a Shimadzu LC−MS/MS 8040 system. The mobile phases used were 20 mM ammonium formate, pH 4.0 ("A") and acetonitrile with 0.1% formic acid ("B"). Analytes were eluted using a 6 min gradient as follows: hold at 90% B (0.5 min), decrease to 40% B (2.00 min), hold at 40% B (4.00 min), increase to 90% B (4.50 min), and hold at 90% B (6.00 min). The injection volume was 5 μL, and the flow rate was set to 0.5 mL/min. The dwell time was 100 ms for every product ion resulting from the 175 m/z (arginine) precursor ion. The 116.05 m/z fragment was used for analysis. Arginine standards (0.48−1000 μM) were prepared in 50 mM bicine, 10 mM NaCl, 50 μM PLP, pH 7.8 and diluted with equal volumes of acetonitrile before being analyzed in the manner just described. The raw counts of the 116.05 m/z fragment were used to build a calibration curve that was used to quantify the amount of 7 produced in the test reactions.

Mass Spectrometry-Based Steady-State Assay. Triplicate reactions (3 × 1 mL) contained 1 mM 7 and 50−12,800 μM L-Orn or L-Gln in 50 mM bicine, 10 mM NaCl, and 50 μM PLP, pH 7.8. The amino donor substrate (L-Orn or L-Gln) concentrations were established by serial dilution. The assays were initiated by the addition of 5 μM ShMppQ. At 5 s intervals up to 30 s, 100 μL aliquots were removed from the reactions and quenched with equal volumes of acetonitrile. The concentrations of arginine at each time point were determined using the same 6 min gradient method described above. Initial rates were determined from the concentration of L-Arg over time, and they were plotted against the initial concentration of amino acid used. GraphPad Prism was used to fit these data to the Michaelis−Menten equation (eq 1) to determine the steady-state kinetic parameters.

RESULTS AND DISCUSSION

Overall Structure of *S. hygroscopicus* MppQ. The crystal structure of ShMppQ with the pyridoxal-5′-phosphate (PLP) cofactor covalently bound (internal aldimine; ShMppQ·PLP) was determined by molecular replacement at a resolution of 1.8 Å (Figure 1). ShMppQ·PLP crystallized in the space

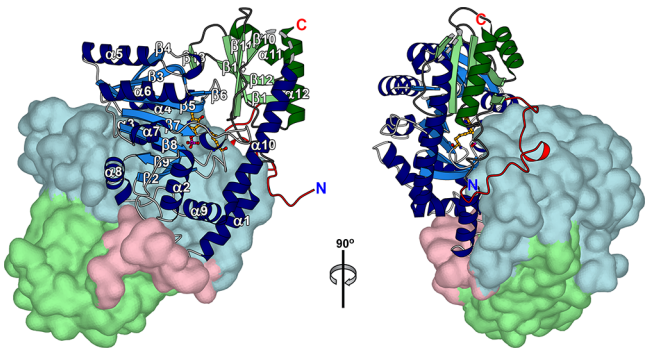

Figure 1. ShMppQ homodimer, with one monomer shown as a ribbon representation and the other shown as a surface representation. The large domain is colored blue, with the helices and strands in dark blue and light blue, respectively. The small domain is colored green, with the same distinction between the secondary structures. The N-terminal extension is colored red.

group $P2_12_12_1$ with unit cell dimensions of a = 47.7, b = 114.5, and c = 133.3 Å and two molecules per asymmetric unit. There are 14 residues at the N-terminus and 12 from the C-terminus of each chain that are not visible in the electron density. Chain B also has a break between residues 323 and 330. Superposition of the two chains using secondary structure matching (SSM),[38] as implemented in COOT, gives a root-mean-square deviation (RMSD) of 0.43 Å for 386 matched Cα atoms. The two chains in the asymmetric unit form a homodimer (Figure 1; 2,974 Å^2 buried surface area) that matches the quaternary structures observed for the known fold-type I aminotransferases.[17,39] Superposition of the ShMppQ dimer onto the *E. coli* aspartate aminotransferase dimer (PDB ID 1ARS[40]) gives an RMSD of 2.85 Å for 620 of the 775 Cα atoms in the ShMppQ·PLP model, highlighting the high degree of quaternary structure similarity between ShMppQ and aspartate aminotransferase.

https://doi.org/10.1021/acs.biochem.3c00428
Biochemistry 2023, 62, 3105−3115

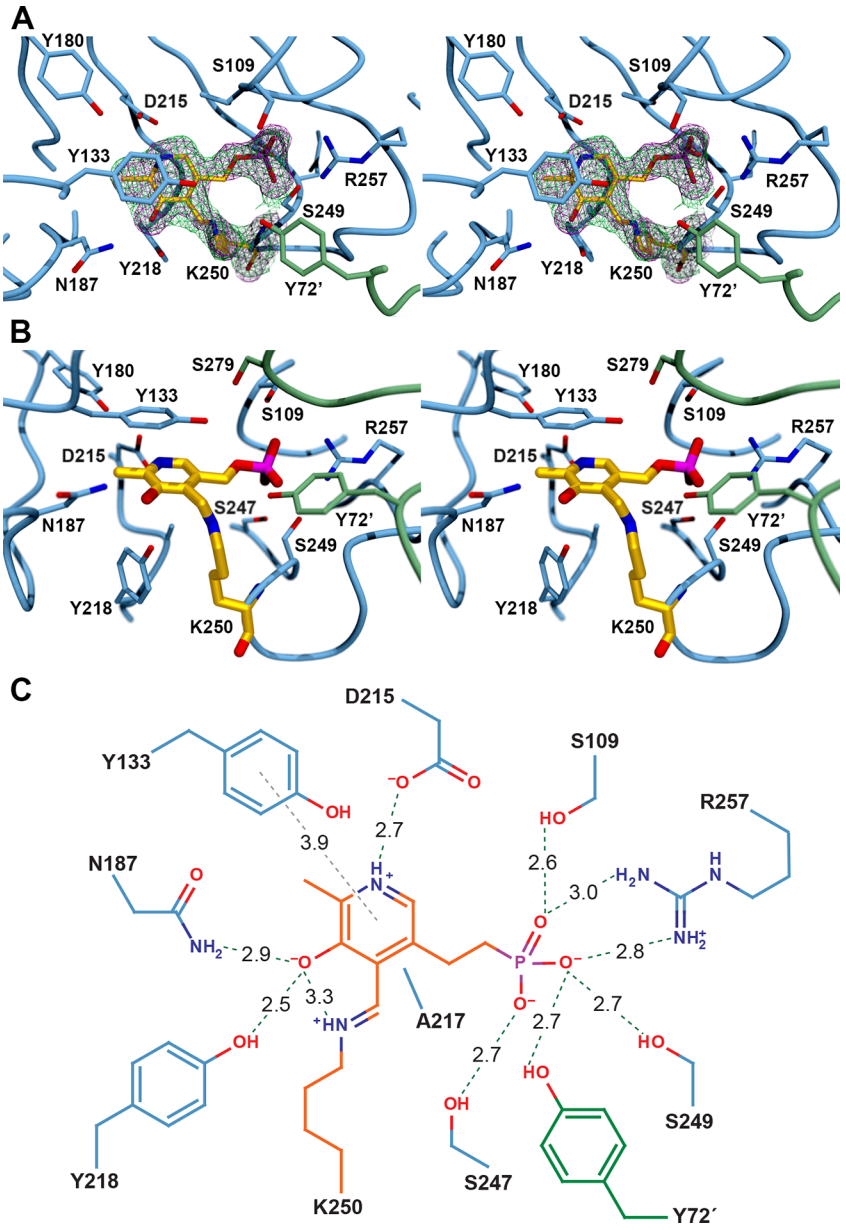

Figure 2. (A) Stereoview of the ShMppQ•PLP active site showing the electron density for the K250-PLP internal aldimine. The $2F_o - F_c$ working map (magenta mesh) and $2F_o - F_c$ simulated annealing composite omit map (green mesh) are contoured at 1.2 σ with a map radius of 2.5 Å. (B) Second stereoview of the active site is shown without electron density and in a different orientation (rotated ~60° in the *x*-axis) to give a clearer picture of the arrangement of amino acids about the cofactor. (C) Schematic representation of the active site showing the interactions of the enzyme with the internal aldimine as dotted lines. The associated distances are given in Å.

The tertiary structure of ShMppQ, like its quaternary structure, matches that of typical fold-type I aminotransferases like L-aspartate aminotransferase.[22,41,42] The fold consists of an N-terminal extension (Met1−Gly35) as well as a large domain (Leu49−Ala324) and a small domain (Val36−Leu48 and Met325−Ser415). The large domain is composed of a seven-stranded mixed β-sheet flanked by 10 α-helices ($\alpha-\beta-\alpha$ sandwich), while the small domain has a mixed $\alpha-\beta$ topology. The large and small domains are linked by a 25-residue long (~40 Å) helix that serves as the "backbone" of the enzyme. The active site is located at the interface between the large domains of each protomer. As in all known fold-type I aminotransferases, the cofactor is held in a cleft between the central β-sheet, and helices α3 and α4 of one subunit, and helix α8 from the other subunit of the dimer (Figure 1).

In addition to the *E. coli* aspartate aminotransferase, a PDBeFold[38,43] search using chain A of the ShMppQ·PLP model returned 388 unique structures having *Q* scores of at least 0.14, the threshold value that implies significant structural similarity.[43] Of these, several had *Q* scores well above 0.4, implying very strong structural similarity.[43] These included the human kynurenine aminotransferase II homologue from *Pyrococcus horikoshii* OT3 (PhKAT-II; PDB ID 1 × 0 M;[24] 30/31% identical, 2.1 Å RMSD), the aromatic amino acid aminotransferase from *Psychrobacter* sp. B6 (PsyArAT; PDB ID 6T3 V;[44] 18/94% identical, 1.9 Å RMSD), and the glutamine−phenylpyruvate aminotransferase from *Thermus thermophilus* HB8 (TtGln *AT*; PDB ID 1 V2D;[45] 27/29% identical, 2.2 Å RMSD). Note that in the sequence identities quoted here, the first number is the traditional, sequence-based

https://doi.org/10.1021/acs.biochem.3c00428
Biochemistry 2023, 62, 3105−3115

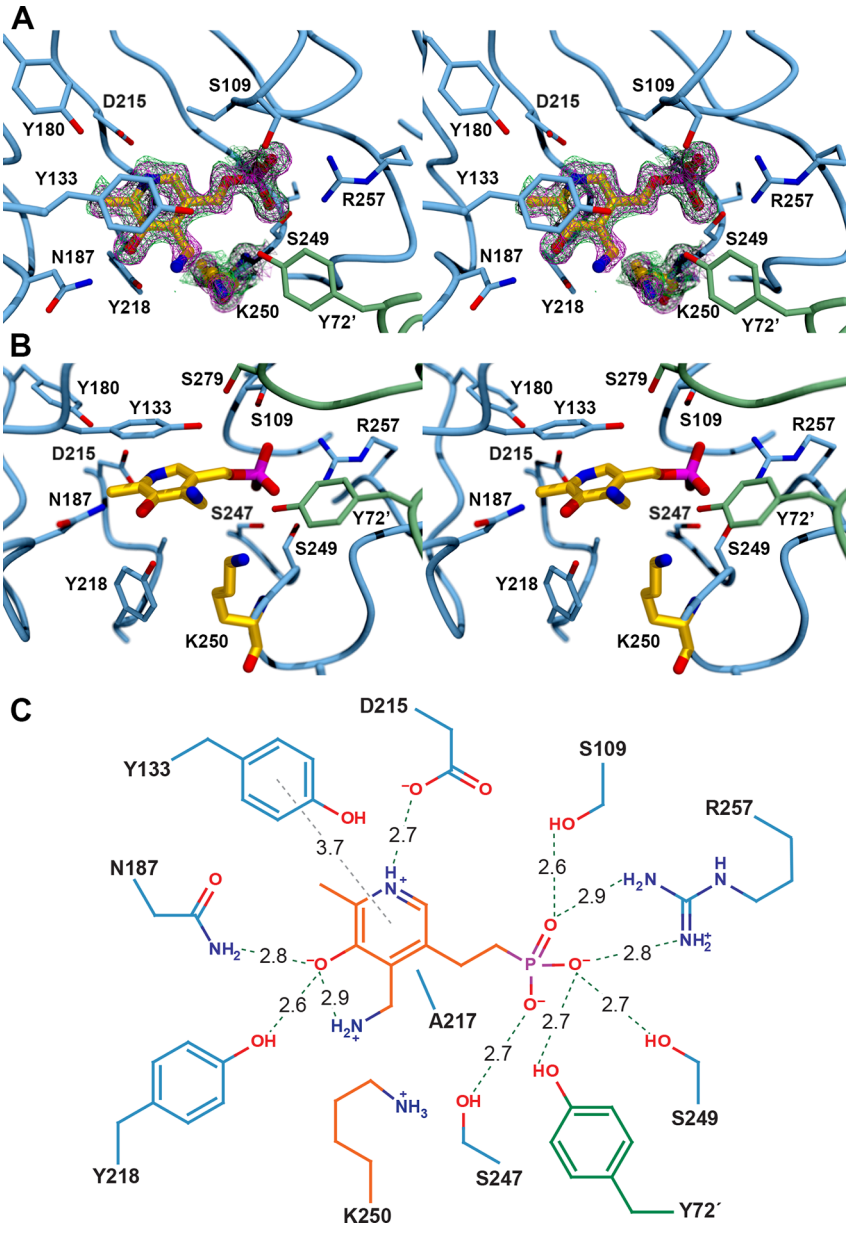

Figure 3. (A) Stereoview of the ShMppQ●PMP active site showing the electron density for catalytic K250 and the PMP cofactor. The $2F_o - F_c$ working map (magenta mesh) and $2F_o - F_c$ simulated annealing composite omit map (green mesh) are contoured at 1.2 σ with a map radius of 2.5 Å. (B) Second stereoview of the active site is shown without the electron density and in a different orientation (rotated ~60° in the *x*-axis) to give a clearer picture of the separation between PMP and K250. (C) Schematic representation of the active site shows the interactions of the active site functional groups with the cofactor, with associated distances in Å.

identity, and the second number is the 3D sequence alignment score generated by PDBeFold.[43] The former catalyzes the production of kynurenic acid and glutamate from kynurenine and α-ketoglutarate,[24] while the latter has been shown to catalyze the glutamine:phenylpyruvate transaminase reaction with a range of aromatic amino acids, including kynurenine.[46]

Comparison of PLP- and PMP-Bound MppQ. The structure of ShMppQ·PLP shows a clear electron density for the covalent attachment of PLP to the catalytic K250 (Figure 2). The side chains surrounding the cofactor are typical of aspartate aminotransferases.[47−50] The side chains of residues N187 and Y218 participate in hydrogen-bonding interactions with the C3 hydroxyl of the cofactor. D215 forms a salt bridge with the pyridinium nitrogen of the cofactor, thus stabilizing it and allowing PLP to act as an electron sink in the reaction with the substrate. The phosphate group of PLP is within the hydrogen-bonding distances of S109, R257, S249, and S247, as well as Y72 of the other protomer (Figure 2). Most side chains lining the active site in the EcAAT active site are identical (Y225, N194, D222, R266, S257, and S255), except for subtle differences (PDB entry: 1ARS).[22] In EcAAT, it is Trp140 that forms interactions with the PLP aromatic ring via pi−pi stacking, while in MppQ, Y133 is found in this location. EcAAT also has T109 interacting with the phosphate moiety instead of S109.

Co-crystallization of the PLP-bound enzyme with 10 mM L-Arg resulted in the trapping of the noncovalent complex between ShMppQ and pyridoxamine-5′-phosphate (PMP). The PMP-bound form of the enzyme was isomorphous with the ShMppQ·PLP complex. These crystals diffracted to 1.6 Å

https://doi.org/10.1021/acs.biochem.3c00428
Biochemistry 2023, 62, 3105−3115

resolution and contained two molecules in the asymmetric unit arranged in the same quaternary structure observed for the PLP-bound form of the enzyme (0.35 Å RMSD for 767 aligned residues). The disordered regions in each chain are identical to those seen in the ShMppQ·PLP model, except chain B of the PMP-bound structure not missing residues A324−G329.

The active site clearly contains PMP, as evidenced by the lack of continuous electron density at K250 (Figure 3). Aside from the presence of PMP in the active site, there is virtually no difference between the active sites of the PLP- and PMP-bound forms of ShMppQ. It will be interesting to find out if the change to a "closed" conformation (rotation of the small domain relative to the large domain) observed in some ATases does not happen in MppQ, or if the crystal simply captured an "open" conformation in each case.

Preliminary Analysis of MppQ Catalytic Activity. The typical transamination reaction begins with the attack of the deprotonated amine of an amino acid on the C4′ imine of PLP to form the external aldimine. Hydrolysis of this adduct releases the keto acid and leaves PMP in the enzyme active site. A different α-keto acid, often α-ketoglutarate, binds to and reacts with PMP, forming a second external aldimine. Given the structural evidence that ShMppQ is an aminotransferase and that it operates in the biosynthesis of L-End from L-Arg, we used steady-state kinetics to assess the reaction of the enzyme with several candidate amino group donor and acceptor substrates.

Since we hypothesized that the in vivo activity of ShMppQ is the transamination of an unknown amino donor substrate with **6** as the amino acceptor substrate, we set out to demonstrate this activity in vitro with L-Ala as the amino donor substrate. Alanine was chosen based on preliminary end-point assays (Figure S4) that demonstrated reasonably efficient transamination activity with L-Arg and pyruvate. The substrate pairs for the reverse (and more physiologically relevant) reaction are L-Ala and **7**. The acceptor substrate **6** was prepared enzymatically using MppP and MppR as described above. Owing to the mixture of **5** and **7** produced by SwMppP, and perhaps inhibition of MppR by **7**, compound **6** produced was estimated to be ∼10% of the reaction mixture. Triplicate reactions were prepared containing a nominal concentration of 50 μM **6** and 100 mM L-Ala in 20 mM TRIS, pH 8.5. The reactions were initiated by the addition of ShMppQ (final concentration of 40 μM). At defined time points, aliquots were taken, quenched with HCl, and then subjected to LC−MS/MS analysis. ShMppQ is able to convert **6** into **1** (Figure 4), using L-Ala as the amino donor substrate.

Difficulties in the preparation of **6** (**7** is a weak inhibitor of ShMppR, and we were unable to purify **6** from residual **5** and **7**) prevented a full steady-state characterization of the reaction with **6**. Therefore, the aminotransferase activity of ShMppQ was tested, with **7** as the amino acceptor substrate and L-Ala as the donor substrate. The reaction was monitored by using a coupled assay with lactate dehydrogenase (LDH). This assay relied on the conversion of L-alanine to pyruvate, which was subsequently reduced to lactate by the LDH coupling enzyme. LDH is an NADH-dependent oxidoreductase, and the consumption of NADH was observed at 340 nm ($\varepsilon_{340\ nm}$ = 6220 M^{-1} cm^{-1}). It was shown that MppQ catalyzes the transamination of **7** and L-alanine efficiently (k_{cat}^{7} = 0.1 ± 0.001 s^{-1}, K_M^{7} = 2.5 ± 0.1 μM, k_{cat}/K_M^{7} = 4.0 ± 0.2 × 10^4 M^{-1} s^{-1}). The low K_M value suggests that ShMppQ has a significant affinity for **7**. It is plausible that this could serve a physiological

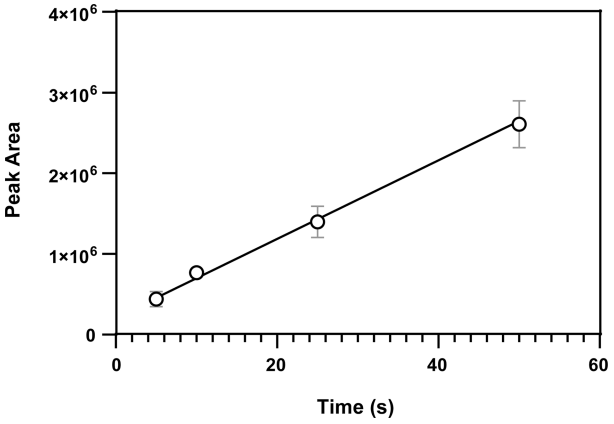

Figure 4. Production of **1** in a reaction of ShMppQ with **6** and L-Ala. The peaks corresponding to all fragments generated from the 173 m/z precursor ion were integrated, and areas under the curve are plotted on the y-axis.

role as it would allow ShMppQ to recycle the off-pathway product of MppP, **7**, back to L-arginine. If this is so, it represents some interesting problem solving by evolution: rather than improving MppP as an oxidase, evolution may have recruited a convenient enzyme in the same pathway to clear up the mess left by MppP.

The last remaining question addressed in this study is that of the physiological amino donor substrate. We sought to answer this question using end-point assays in which ShMppQ was incubated with a saturating concentration of **7** and a panel of potential amino donor substrates. The donor substrates tested included L-His, L-Gln, L-Orn, L-Lys, L-canavanine, L-Ala, L-Thr, L-Ile, L-Phe, L-Asp, and L-Glu. The first three were chosen based on their rough similarity to **6** in terms of size and polarity. Lysine and canavanine were tested due to their similarity to arginine. Alanine was tested as a positive control since it was already a known (though poor) substrate. Threonine, isoleucine, and phenylalanine were chosen due to the similarity of ShMppQ to some aromatic and branched-chain amino acid aminotransferases. Likewise, aspartate and glutamate were selected due to the similarity of ShMppQ to aspartate aminotransferases. Aliquots were taken from each reaction mixture at 5 and 10 min, and arginine produced at each time point was quantified by LC−MS/MS. L-Ornithine was the most efficient donor substrate (Table 2). It produced the greatest amount of L-Arg (∼580 μM), converting over half of the starting material, **7**. While the two time points tested do not give quantitative rate information, they do give a qualitative sense of the velocities of the reactions. The reaction with ornithine as the donor substrate had reached its equilibrium concentration of L-Arg at or before 5 min. In contrast, the reaction with L-Lys as the donor substrate produced the next highest amount of L-Arg (∼490 μM), turning over about half of the starting material, but had only produced ∼230 μM L-Arg after 5 min. Clearly, this is a slower reaction. It should be noted that the equilibria of the reactions with L-Orn and L-Lys as the amino donor substrates lie further toward the product because both keto acids cyclize to give a five- or a six-membered ring, respectively. ShMppQ also produced a significant amount of L-Arg after 10 min, with L-Gln as the donor substrate (∼320 μM), but again, this reaction was still slower than the reaction with ornithine but was faster than the reaction with L-Lys. Both L-histidine and L-canavanine

https://doi.org/10.1021/acs.biochem.3c00428
Biochemistry 2023, 62, 3105−3115

Table 2. Concentrations (μM) of L-Arg (3) Produced at Two Time Points by 5 μM ShMppQ from a Saturating Concentration (1 mM) of the Amino Acceptor Substrate 2-Ketoarginine (7) in Assays with 1 mM L-His, L-Gln, L-Orn, L-Lys, L-Canavanine, L-Ala, L-Thr, L-Ile, L-Phe, L-Asp, or L-Glu as the Amino Donor Substrate in 50 mM Bicine, 10 mM NaCl, 50 μM PLP, pH 7.8[a]

	reaction time	
amino group donor	5 min	10 min
L-His	54 ± 3.9	80 ± 1.0
L-Gln	288 ± 6.1	319 ± 7.8
L-Orn	579 ± 11.6	556 ± 18.2
L-Lys	228 ± 22.5	487 ± 28.2
L-Canavanine	59 ± 1.9	154 ± 16.3
L-Ala	2 ± 0.2	3 ± 0.5
L-Thr	ND	ND
L-Ile	ND	ND
L-Phe	ND	ND
L-Asp	9 ± 1.3	6 ± 1.2
L-Glu	ND	ND

[a]ND = none detected.

were relatively poor substrates, converting only 10 or 15%, respectively, of the starting material to L-Arg after 10 min. L-Asp was the only other donor substrate tested that appeared to plateau by the 5 min time point. However, it converted less than 1% of **7** in the reaction to L-Arg, putting aspartate on par with alanine as an extremely poor donor substrate. Two final points should be noted. First, this analysis of the donor substrate preference is complicated by the fact that these are end-point assays and that the reactions have come to equilibrium. The relative amounts of L-Arg produced from **7** may reflect the thermodynamic stabilities of the corresponding amino- and keto-acids produced. Second, it is possible, though perhaps not likely, that the physiological amino donor substrate is L-Arg. This is unlikely because L-canavanine is expected to behave similar to L-Arg, and L-canavanine is a poor amino donor substrate according to the end-point assay results. Still, this possibility cannot be ruled out until a means of obtaining pure **6** can be devised.

Though ornithine clearly outperformed the other donor substrates tested, there are few PLP-dependent transaminases that work on ornithine. Ornithine aminotransferase (OAT; EC 2.6.1.13), which is found in all divisions of life, is a δ-aminotransferase that produces glutamate-5-semialdehyde in proline metabolism.[51] There is somewhat more precedent for glutamine α-aminotransferases, including glutamine–phenylpyruvate transaminase (EC 2.6.1.15; 1 V2D),[45] glutamine-scyllo-inositol transaminase (EC 2.6.1.50; 7B0D),[52] and glutamine:2-deoxy-scyllo-inosose aminotransferase (EC 2.6.1.100; 2C81).[53] The transamination of 2-ketoenduracididine (**6**) and glutamine is analogous to the reaction of the structurally homologous glutamine:phenylpyruvate aminotransferase from *T. thermophilus* HB8. This is interesting because, while the glutamine transaminase activity is widespread in eukaryotes,[54] the *T. thermophilus* enzyme was the first, and at this time still the only, example of a prokaryotic glutamine transaminase.[46]

Thus, we examined the steady- state kinetics of ShMppQ with both L-Orn and L-Gln as amino donor substrates and **7** as the amino acceptor substrate. Our findings indicate that there is no significant difference between ornithine and glutamine in terms of their ability to act as amino donors for the ShMppQ-catalyzed transamination of **6** to L-End (**1**). The kinetic constants are all essentially identical (Table 3), so it is difficult

Table 3. Steady-State Kinetics of Transamination of 7 and L-Orn or L-Gln by 5 μM ShMppQ in 50 mM Bicine, 10 mM NaCl, 50 μM PLP, pH 7.8, 25 °C

	L-Orn	L-Gln
V_{max} (μM·s^{-1})	10.3 ± 0.4	2.3 ± 0.2
k_{cat} (s^{-1})	2.1 ± 0.1	0.5 ± 0.04
K_M (μM)	434 ± 51.9	368 ± 136
k_{cat}/K_M (M^{-1} s^{-1})	(4.8 ± 0.6) × 10^3	(1.4 ± 0.5) × 10^3

to identify either as a physiological amino donor substrate. Perhaps, the relative concentrations of ornithine and glutamine in cells could provide a clue. The intracellular concentration of L-Orn is estimated to be quite low, in the range of 20–30 μM in human (hepatoma) cells[55] and (0.2–0.6 μmol g^{-1} FW) in *Arabidopsis thaliana*.[56] Intracellular glutamine concentrations are considerably higher. For example, in *Salmonella typhimurium*, the intracellular concentration of glutamine is estimated to be ∼3 mM.[57] Based on the likelihood that glutamine is up to 100-fold more abundant than ornithine, glutamine is the most plausible candidate for the physiological amino donor substrate. This detailed structural and functional characterization of ShMppQ completes the elucidation of the L-End biosynthetic pathway.

■ ASSOCIATED CONTENT

Supporting Information

The Supporting Information is available free of charge at https://pubs.acs.org/doi/10.1021/acs.biochem.3c00428.

Liquid chromatography–mass spectrometry chromatograms of enzymatically produced mixture of **5** and **7** and of enzymatically produced **6 and** NMR spectra of enzymatically produced **7** (PDF)

Accession Codes

ShMppQ, Q643B9.

■ AUTHOR INFORMATION

Corresponding Author

Nicholas R. Silvaggi − *Department of Chemistry and Biochemistry, University of Wisconsin-Milwaukee, Milwaukee, Wisconsin 53211, United States;* orcid.org/0000-0003-0576-0714; Phone: 414-229-2647; Email: silvaggi@uwm.edu

Authors

Nemanja Vuksanovic − *Department of Chemistry and Biochemistry, University of Wisconsin-Milwaukee, Milwaukee, Wisconsin 53211, United States; Department of Chemistry, Boston University, Boston, Massachusetts 02215, United States*

Trevor R. Melkonian − *Department of Chemistry and Biochemistry, University of Wisconsin-Milwaukee, Milwaukee, Wisconsin 53211, United States; Division of Chemical Biology and Medicinal Chemistry, The University of Texas at Austin, Austin, Texas 78712, United States*

Dante A. Serrano − *Department of Chemistry and Biochemistry, University of Wisconsin-Milwaukee, Milwaukee, Wisconsin 53211, United States; Department of Chemistry,*

https://doi.org/10.1021/acs.biochem.3c00428
Biochemistry 2023, 62, 3105−3115

Pennsylvania State University, University Park, Pennsylvania 16802, United States; orcid.org/0000-0001-7084-1479

Alan W. Schwabacher − *Department of Chemistry and Biochemistry, University of Wisconsin-Milwaukee, Milwaukee, Wisconsin 53211, United States;* orcid.org/0000-0003-4984-1276

Complete contact information is available at: https://pubs.acs.org/10.1021/acs.biochem.3c00428

Author Contributions

⊥N.V. and T.R.M. are co-first authors.

Author Contributions

The manuscript was written through contributions of all authors. All authors have given approval to the final version of the manuscript.

Funding

This work was supported by grant CHE-1903899 from the National Science Foundation, Division of Chemistry.

Notes

The authors declare no competing financial interest.

■ ACKNOWLEDGMENTS

This work was funded by grant number CHE-1903899 from the National Science Foundation, Division of Chemistry. This research used resources of the Advanced Photon Source, a U.S. Department of Energy (DOE) Office of Science User Facility operated for the DOE Office of Science by Argonne National Laboratory under contract no. DE-AC02-06CH11357. Use of the LS-CAT Sector 21 was supported by the Michigan Economic Development Corporation and the Michigan Technology Tri-Corridor (Grant 085P1000817).

■ ABBREVIATION

ShMppQ, *Streptomyces hygroscopicus* MppQ

■ REFERENCES

(1) Fang, X.; Tiyanont, K.; Zhang, Y.; Wanner, J.; Boger, D.; Walker, S. The mechanism of action of ramoplanin and enduracidin. *Mol. Biosyst.* **2006**, *2*, 69−76.

(2) Magarvey, N. A.; Haltli, B.; He, M.; Greenstein, M.; Hucul, J. A. Biosynthetic pathway for mannopeptimycins, lipoglycopeptide antibiotics active against drug-resistant gram-positive pathogens. *Antimicrob. Agents Chemother.* **2006**, *50*, 2167−2177.

(3) Wu, M. C.; Styles, M. Q.; Law, B. J.; Struck, A. W.; Nunns, L.; Micklefield, J. Engineered biosynthesis of enduracidin lipoglycopeptide antibiotics using the ramoplanin mannosyltransferase Ram29. *Microbiology* **2015**, *161*, 1338−1347.

(4) Petersen, P. J.; Wang, T. Z.; Dushin, R. G.; Bradford, P. A. Comparative in vitro activities of AC98−6446, a novel semisynthetic glycopeptide derivative of the natural product mannopeptimycin alpha, and other antimicrobial agents against gram-positive clinical isolates. *Antimicrob. Agents Chemother.* **2004**, *48*, 739−746.

(5) Atkinson, D. J.; Naysmith, B. J.; Furkert, D. P.; Brimble, M. A. Enduracididine, a rare amino acid component of peptide antibiotics: Natural products and synthesis. *Beilstein J. Org. Chem.* **2016**, *12*, 2325−2342.

(6) Craig, W.; Chen, J.; Richardson, D.; Thorpe, R.; Yuan, Y. A Highly Stereoselective and Scalable Synthesis of L-allo-Enduracididine. *Org. Lett.* **2015**, *17*, 4620−4623.

(7) Olivier, K. S.; Van Nieuwenhze, M. S. Synthetic studies toward the mannopeptimycins: synthesis of orthogonally protected beta-hydroxyenduracididines. *Org. Lett.* **2010**, *12*, 1680−1683.

(8) Hatano, K.; Nogami, I.; Higashide, E.; Kishi, T. Biosynthesis of Enduracidin: Origin of Enduracididine and Other Amino Acids. *Agric. Biol. Chem.* **1984**, *48*, 1503−1508.

(9) Ruzin, A.; Singh, G.; Severin, A.; Yang, Y.; Dushin, R. G.; Sutherland, A. G.; Minnick, A.; Greenstein, M.; May, M. K.; Shlaes, D. M.; Bradford, P. A. Mechanism of action of the mannopeptimycins, a novel class of glycopeptide antibiotics active against vancomycin-resistant gram-positive bacteria. *Antimicrob. Agents Chemother.* **2004**, *48*, 728−738.

(10) Yin, X.; Zabriskie, T. M. The enduracidin biosynthetic gene cluster from Streptomyces fungicidicus. *Microbiology* **2006**, *152*, 2969−2983.

(11) Goebel, N. C. Biosynthesis and Modification of the Antibiotic Enduracidin. In *School of Pharmacy*; Oregon State University, 2012.

(12) Yin, X.; Zabriskie, T. M. VioC is a non-heme iron, alpha-ketoglutarate-dependent oxygenase that catalyzes the formation of 3S-hydroxy-L-arginine during viomycin biosynthesis. *ChemBioChem* **2004**, *5*, 1274−1277.

(13) Yin, X.; McPhail, K. L.; Kim, K. J.; Zabriskie, T. M. Formation of the nonproteinogenic amino acid 2S,3R-capreomycidine by VioD from the viomycin biosynthesis pathway. *ChemBioChem* **2004**, *5*, 1278−1281.

(14) Han, L.; Schwabacher, A. W.; Moran, G. R.; Silvaggi, N. R. *Streptomyces wadayamensis* MppP is a pyridoxal 5′-phosphate-dependent L-arginine α-deaminase, γ-hydroxylase in the enduracididine biosynthetic pathway. *Biochemistry* **2015**, *54*, 7029−7040.

(15) Han, L.; Vuksanovic, N.; Oehm, S. A.; Fenske, T. G.; Schwabacher, A. W.; Silvaggi, N. R. *Streptomyces wadayamensis* MppP is a PLP-dependent oxidase, not an oxygenase. *Biochemistry* **2018**, *57*, 3252−3264.

(16) Burroughs, A. M.; Hoppe, R. W.; Goebel, N. C.; Sayyed, B. H.; Voegtline, T. J.; Schwabacher, A. W.; Zabriskie, T. M.; Silvaggi, N. R. Structural and functional characterization of MppR, an enduracididine biosynthetic enzyme from streptomyces hygroscopicus: functional diversity in the acetoacetate decarboxylase-like superfamily. *Biochemistry* **2013**, *52*, 4492−4506.

(17) Eliot, A. C.; Kirsch, J. F. Pyridoxal phosphate enzymes: mechanistic, structural, and evolutionary considerations. *Annu. Rev. Biochem.* **2004**, *73*, 383−415.

(18) Toney, M. D. Controlling reaction specificity in pyridoxal phosphate enzymes. *Biochim. Biophys. Acta* **2011**, *1814*, 1407−1418.

(19) Christen, P.; Mehta, P. K. From cofactor to enzymes. The molecular evolution of pyridoxal-5′-phosphate-dependent enzymes. *Chem. Rec.* **2001**, *1*, 436−447.

(20) Mehta, P. K.; Christen, P. The molecular evolution of pyridoxal-5′-phosphate-dependent enzymes. *Adv. Enzymol. Relat. Areas Mol. Biol.* **2000**, *74*, 129−184.

(21) Percudani, R.; Peracchi, A. A genomic overview of pyridoxal-phosphate-dependent enzymes. *EMBO reports* **2003**, *4*, 850−854.

(22) Jager, J.; Moser, M.; Sauder, U.; Jansonius, J. N. Crystal structures of Escherichia coli aspartate aminotransferase in two conformations. Comparison of an unliganded open and two liganded closed forms. *J. Mol. Biol.* **1994**, *239*, 285−305.

(23) Jager, J.; Pauptit, R. A.; Sauder, U.; Jansonius, J. N. Three-dimensional structure of a mutant E. coli aspartate aminotransferase with increased enzymic activity. *Protein Eng.* **1994**, *7*, 605−612.

(24) Chon, H.; Matsumura, H.; Koga, Y.; Takano, K.; Kanaya, S. Crystal structure of a human kynurenine aminotransferase II homologue from Pyrococcus horikoshii OT3 at 2.20 A resolution. *Proteins* **2005**, *61*, 685−688.

(25) Battye, T. G.; Kontogiannis, L.; Johnson, O.; Powell, H. R.; Leslie, A. G. iMOSFLM: a new graphical interface for diffraction-image processing with MOSFLM. *Acta Crystallogr., Sect. D: Biol. Crystallogr.* **2011**, *67*, 271−281.

(26) Evans, P. Scaling and assessment of data quality. *Acta Crystallogr., Sect. D: Biol. Crystallogr.* **2006**, *62*, 72−82.

(27) Winn, M. D.; Ballard, C. C.; Cowtan, K. D.; Dodson, E. J.; Emsley, P.; Evans, P. R.; Keegan, R. M.; Krissinel, E. B.; Leslie, A. G.; McCoy, A.; McNicholas, S. J.; Murshudov, G. N.; Pannu, N. S.;

Potterton, E. A.; Powell, H. R.; Read, R. J.; Vagin, A.; Wilson, K. S. Overview of the CCP4 suite and current developments. *Acta Crystallogr., Sect. D: Biol. Crystallogr.* **2011**, *67*, 235−242.
(28) Vonrhein, C.; Flensburg, C.; Keller, P.; Sharff, A.; Smart, O.; Paciorek, W.; Womack, T.; Bricogne, G. Data processing and analysis with the autoPROC toolbox. *Acta Crystallogr., Sect. D: Biol. Crystallogr.* **2011**, *67*, 293−302.
(29) McCoy, A. J.; Grosse-Kunstleve, R. W.; Adams, P. D.; Winn, M. D.; Storoni, L. C.; Read, R. J. Phaser crystallographic software. *J. Appl. Crystallogr.* **2007**, *40*, 658−674.
(30) Adams, P. D.; Afonine, P. V.; Bunkoczi, G.; Chen, V. B.; Davis, I. W.; Echols, N.; Headd, J. J.; Hung, L. W.; Kapral, G. J.; Grosse-Kunstleve, R. W.; McCoy, A. J.; Moriarty, N. W.; Oeffner, R.; Read, R. J.; Richardson, D. C.; Richardson, J. S.; Terwilliger, T. C.; Zwart, P. H. PHENIX: a comprehensive Python-based system for macromolecular structure solution. *Acta Crystallogr., Sect. D: Biol. Crystallogr.* **2010**, *66*, 213−221.
(31) Terwilliger, T. C.; Grosse-Kunstleve, R. W.; Afonine, P. V.; Moriarty, N. W.; Zwart, P. H.; Hung, L. W.; Read, R. J.; Adams, P. D. Iterative model building, structure refinement and density modification with the PHENIX AutoBuild wizard. *Acta Crystallogr., Sect. D: Biol. Crystallogr.* **2008**, *64*, 61−69.
(32) Zwart, P. H.; Afonine, P. V.; Grosse-Kunstleve, R. W.; Hung, L. W.; Ioerger, T. R.; McCoy, A. J.; McKee, E.; Moriarty, N. W.; Read, R. J.; Sacchettini, J. C.; Sauter, N. K.; Storoni, L. C.; Terwilliger, T. C.; Adams, P. D. Automated structure solution with the PHENIX suite. *Methods Mol. Biol.* **2008**, *426*, 419−435.
(33) Afonine, P. V.; Mustyakimov, M.; Grosse-Kunstleve, R. W.; Moriarty, N. W.; Langan, P.; Adams, P. D. Joint X-ray and neutron refinement with phenix.refine. *Acta Crystallogr., Sect. D: Biol. Crystallogr.* **2010**, *66*, 1153−1163.
(34) Emsley, P.; Cowtan, K. Coot: model-building tools for molecular graphics. *Acta Crystallogr., Sect. D: Biol. Crystallogr.* **2004**, *60*, 2126−2132.
(35) Emsley, P.; Lohkamp, B.; Scott, W. G.; Cowtan, K. Features and development of Coot. *Acta Crystallogr., Sect. D: Biol. Crystallogr.* **2010**, *66*, 486−501.
(36) Meister, A. The alpha-keto analogues of arginine, ornithine, and lysine. *J. Biol. Chem.* **1954**, *206*, 577−585.
(37) Stalon, V.; Mercenier, A. L-arginine utilization by Pseudomonas species. *J. Gen. Microbiol.* **1984**, *130*, 69−76.
(38) Krissinel, E.; Henrick, K. Secondary-structure matching (SSM), a new tool for fast protein structure alignment in three dimensions. *Acta Crystallogr., Sect. D: Biol. Crystallogr.* **2004**, *60*, 2256−2268.
(39) Schneider, G.; Kack, H.; Lindqvist, Y. The manifold of vitamin B6 dependent enzymes. *Structure* **2000**, *8*, R1−R6.
(40) Okamoto, A.; Higuchi, T.; Hirotsu, K.; Kuramitsu, S.; Kagamiyama, H. X-ray crystallographic study of pyridoxal 5′-phosphate-type aspartate aminotransferases from Escherichia coli in open and closed form. *J. Biochem.* **1994**, *116*, 95−107.
(41) Schwarzenbacher, R.; Jaroszewski, L.; von Delft, F.; Abdubek, P.; Ambing, E.; Biorac, T.; Brinen, L. S.; Canaves, J. M.; Cambell, J.; Chiu, H. J.; Dai, X.; Deacon, A. M.; DiDonato, M.; Elsliger, M. A.; Eshagi, S.; Floyd, R.; Godzik, A.; Grittini, C.; Grzechnik, S. K.; Hampton, E.; Karlak, C.; Klock, H. E.; Koesema, E.; Kovarik, J. S.; Kreusch, A.; Kuhn, P.; Lesley, S. A.; Levin, I.; McMullan, D.; McPhillips, T. M.; Miller, M. D.; Morse, A.; Moy, K.; Ouyang, J.; Page, R.; Quijano, K.; Robb, A.; Spraggon, G.; Stevens, R. C.; van den Bedem, H.; Velasquez, J.; Vincent, J.; Wang, X.; West, B.; Wolf, G.; Xu, Q.; Hodgson, K. O.; Wooley, J.; Wilson, I. A. Crystal structure of an aspartate aminotransferase (TM1255) from Thermotoga maritima at 1.90 A resolution. *Proteins* **2004**, *55*, 759−763.
(42) Son, H. F.; Kim, K. J. Structural Insights into a Novel Class of Aspartate Aminotransferase from Corynebacterium glutamicum. *PLoS One* **2016**, *11*, No. e0158402.
(43) Krissinel, E.; Henrick, K. Multiple Alignment of Protein Structures in Three Dimensions. In *Computational Life Sciences*; Berthold, M. R., Glen, R. C., Diederichs, K., Kohlbacher, O., Fischer, I., Eds.; Springer Berlin Heidelberg: Berlin, Heidelberg, 2005; pp 67−78.
(44) Bujacz, A.; Rum, J.; Rutkiewicz, M.; Pietrzyk-Brzezinska, A. J.; Bujacz, G. Structural Evidence of Active Site Adaptability towards Different Sized Substrates of Aromatic Amino Acid Aminotransferase from Psychrobacter Sp. B6. *Materials* **2021**, *14*, 3351.
(45) Goto, M.; Omi, R.; Miyahara, I.; Hosono, A.; Mizuguchi, H.; Hayashi, H.; Kagamiyama, H.; Hirotsu, K. Crystal structures of glutamine:phenylpyruvate aminotransferase from Thermus thermophilus HB8: induced fit and substrate recognition. *J. Biol. Chem.* **2004**, *279*, 16518−16525.
(46) Hosono, A.; Mizuguchi, H.; Hayashi, H.; Goto, M.; Miyahara, I.; Hirotsu, K.; Kagamiyama, H. Glutamine:phenylpyruvate aminotransferase from an extremely thermophilic bacterium, Thermus thermophilus HB8. *J. Biochem.* **2003**, *134*, 843−851.
(47) Ford, G. C.; Eichele, G.; Jansonius, J. N. Three-dimensional structure of a pyridoxal-phosphate-dependent enzyme, mitochondrial aspartate aminotransferase. *Proc. Natl. Acad. Sci. U. S. A.* **1980**, *77*, 2559−2563.
(48) Goldberg, J. M.; Swanson, R. V.; Goodman, H. S.; Kirsch, J. F. The tyrosine-225 to phenylalanine mutation of Escherichia coli aspartate aminotransferase results in an alkaline transition in the spectrophotometric and kinetic pKa values and reduced values of both kcat and Km. *Biochemistry* **1991**, *30*, 305−312.
(49) Mollova, E. T.; Metzler, D. E.; Kintanar, A.; Kagamiyama, H.; Hayashi, H.; Hirotsu, K.; Miyahara, I. Use of < sup > 1</sup > H−<sup > 15</sup > N Heteronuclear Multiple-Quantum Coherence NMR Spectroscopy To Study the Active Site of Aspartate Aminotransferase. *Biochemistry* **1997**, *36*, 615−625.
(50) Yano, T.; Kuramitsu, S.; Tanase, S.; Morino, Y.; Kagamiyama, H. Role of Asp222 in the catalytic mechanism of Escherichia coli aspartate aminotransferase: the amino acid residue which enhances the function of the enzyme-bound coenzyme pyridoxal 5′-phosphate. *Biochemistry* **1992**, *31*, 5878−5887.
(51) Shen, B. W.; Hennig, M.; Hohenester, E.; Jansonius, J. N.; Schirmer, T. Crystal structure of human recombinant ornithine aminotransferase. *J. Mol. Biol.* **1998**, *277*, 81−102.
(52) Lucher, L. A.; Chen, Y. M.; Walker, J. B. Reactions catalyzed by purified L-glutamine: keto-scyllo-inositol aminotransferase, an enzyme required for biosynthesis of aminocyclitol antibiotics. *Antimicrob. Agents Chemother.* **1989**, *33*, 452−459.
(53) Popovic, B.; Tang, X.; Chirgadze, D. Y.; Huang, F.; Blundell, T. L.; Spencer, J. B. Crystal structures of the PLP- and PMP-bound forms of BtrR, a dual functional aminotransferase involved in butirosin biosynthesis. *Proteins* **2006**, *65*, 220−230.
(54) Cooper, A. J.; Shurubor, Y. I.; Dorai, T.; Pinto, J. T.; Isakova, E. P.; Deryabina, Y. I.; Denton, T. T.; Krasnikov, B. F. omega-Amidase: an underappreciated, but important enzyme in L-glutamine and L-asparagine metabolism; relevance to sulfur and nitrogen metabolism, tumor biology and hyperammonemic diseases. *Amino Acids* **2016**, *48*, 1−20.
(55) Wu, V. S.; Byus, C. V. A role for ornithine in the regulation of putrescine accumulation and ornithine decarboxylase activity in Reuber H35 hepatoma cells. *Biochim. Biophys. Acta* **1984**, *804*, 89−99.
(56) Majumdar, R.; Shao, L.; Minocha, R.; Long, S.; Minocha, S. C. Ornithine: the overlooked molecule in the regulation of polyamine metabolism. *Plant Cell Physiol.* **2013**, *54*, 990−1004.
(57) Ikeda, T. P.; Shauger, A. E.; Kustu, S. Salmonella typhimurium apparently perceives external nitrogen limitation as internal glutamine limitation. *J. Mol. Biol.* **1996**, *259*, 589−607.

https://doi.org/10.1021/acs.biochem.3c00428
Biochemistry 2023, 62, 3105−3115